JOURNAL OF MATERIALS SCIENCE 10 (1975) 578–588

The tensile deformation of unidirectionally solidified Al–Al_3Ni and Al–Al_2Cu eutectics

B. CANTOR*, G. A. CHADWICK†
Department of Metallurgy and Materials Science, University of Cambridge, UK

Transmission electron microscopy has been used to investigate the dislocation structures produced in single crystals of Al–Al_3Ni and Al–Al_2Cu eutectics deformed in tension. Matrix dislocation densities in the as-grown eutectics are very high, owing to differential thermal contraction effects. The subsequent deformation behaviour of the eutectic crystals is shown to be controlled by the initial high dislocation density, and a constraint effect due to the presence of closely spaced fibres or lamellae.

1. Introduction

The bulk mechanical properties and fracture behaviour of directionally solidified eutectic alloys have been studied extensively (for recent examples see [1-3]). In contrast, deformation mechanisms in eutectics have received very little attention, although dislocation sub-boundaries have been reported to form in Al–Al_3Ni deformed in tension [4] and creep [5], and Al–Al_2Cu deformed in compression [6]. In the present work, the tensile deformation of aligned Al–Al_3Ni and Al–Al_2Cu eutectic single crystals was investigated at several temperatures. Crystallographic effects of deformation were studied by a combination of X-ray and electron diffraction techniques, and the micromechanics of deformation were studied by direct observation of dislocation and surface slip-line structures, using transmission and replication electron metallography.

2. Experimental procedure

Alloys of eutectic composition were made up from aluminium of 99.998% purity and copper and nickel of 99.999% purity. They were melted under argon in recrystallized alumina crucibles and cast into long flat ingots of rectangular cross-section. These ingots were placed individually in a closed graphite mould, enclosed in a silica tube, and directionally solidified under argon in a travelling annular resistance furnace. Solidification was up a slight gradient in order to produce a head of liquid metal to keep the mould filled.

Single crystals were grown by a melt-back technique [7] in which the ingots were solidified in one direction, reversed in the mould, all but the tail end remelted, and re-solidified using the tail end as a seed. This was repeated several times until a single crystal resulted from competitive grain growth, typically requiring three or four passes. The Al–Al_3Ni eutectic was grown at 110 mm h^{-1} and contained Al_3Ni fibres of spacing 1.2 $\pm$ 0.2 μm; the Al–Al_2Cu eutectic was grown at 40 mm h^{-1} and had a lamellar spacing of 2.8 $\pm$ 0.3 μm. There were no bands of structural inhomogeneity in any of the crystals.

Kikuchi-line electron diffraction techniques were used to determine the crystallography of aligned Al–Al_3Ni and Al–Al_2Cu eutectic single crystals. The results are described in detail elsewhere [8]. The crystallography of each of the six Al–Al_3Ni crystals selected for tensile testing was within $\pm$ 2° to 3° of one of the following orientation relationships:

1. $\{001\}_{Al_3Ni}$ // $\{331\}_{Al}$
   $\langle 010\rangle_{Al_3Ni}$ // $\langle 110\rangle_{Al}$ // fibre axis // growth direction
2. $\{102\}_{Al_3Ni}$ // $\{111\}_{Al}$
   $\langle 010\rangle_{Al_3Ni}$ // $\langle 321\rangle_{Al}$ // fibre axis // growth direction
3. $\{102\}_{Al_3Ni}$ // $\{001\}_{Al}$
   $\langle 010\rangle_{Al_3Ni}$ // $\langle 210\rangle_{Al}$ // fibre axis and 7° to 8° away from the growth direction.

The crystallography of each of the four Al–Al_2Cu

*Present address: Applied Sciences Laboratory, University of Sussex, Falmer, Brighton, Sussex, UK.
†Present address: Department of Mining and Metallurgical Engineering, University of Queensland, St. Lucia, Brisbane, Australia.

crystals selected for tensile testing was within $\pm$ 8° to 10° of:

$\{211\}_{Al_2Cu}$ // $\{111\}_{Al}$ // lamellar interface
$\langle 120\rangle_{Al_2Cu}$ // $\langle 110\rangle_{Al}$

growth direction // high index vector of each phase.

Eight tensile specimens were cut from each eutectic crystal by trepanning the gauge length profile with a shaped tool on a spark machine. The use of a crystal goniometer ensured that in all cases the gauge length was parallel to the growth direction. The gauge length was typically 12.5 mm with a square cross-section 3.0 mm by 3.0 mm. To remove surface damage, the Al–Al_3Ni tensile specimens were electropolished at 233 K and 15 V in 80/20 methanol/perchloric acid; the Al–Al_2Cu specimens were electropolished at 233 K and 12 V in 90/10 methanol/nitric acid.

Tensile specimens of Al–Al_3Ni were tested at 293, 593 and 743 K; tensile specimens of Al-Al_2Cu were tested at 293, 593 and 723 K. Specimens with each of the three Al–Al_3Ni crystallographic orientations were tested at each temperature. Tensile testing was carried out in air using an Instron TM testing machine, with a furnace enclosing specimen and grips. The system equilibrated at all temperatures within 30 min and tests were performed as soon as the temperature had stabilized. After testing, specimens had cooled to room temperature within 10 min. In the room temperature tests, the strain was measured directly with a Wiedemann-Baldwin microformer-type extensometer; in the high temperature tests, strain was measured indirectly from the cross-head movement by making a correction for machine compliance, calculated from the room temperature tests. In all tests the strain rate was 1.25% min^{-1}. One specimen from each crystal was not tested and used as a control specimen. Of the remaining seven specimens from each crystal, two were tested to fracture and five were deformed to various strains and then unloaded.

Before and after tensile testing, the relative orientations of the aluminium phase and growth direction of each Al–Al_3Ni specimen was determined in a conventional back-reflection Läue X-ray camera. A crystal goniometer specimen stage was used to ensure precise realignment of each specimen before and after testing. This procedure enabled the investigation of any crystallographic rotation of the tensile axis during deformation.

Before and after tensile testing, two-stage plastic-carbon replicas were taken from the gauge length surface of each specimen. The replicas were shadowed with 99.999% purity gold, and examined in an A.E.I. EM6G electron microscope at 80 kV.

Discs, 3 mm diameter and 1 mm thick, were spark-machined from each deformed specimen and from each control specimen. In all Al–Al_2Cu specimens, discs were spark-machined transverse to the tensile axis; in the Al–Al_3Ni specimens, discs were spark-machined both transverse to the tensile axis, and parallel to the primary slip plane of the aluminium phase. For each Al–Al_3Ni specimen, the orientation of the primary slip plane had been determined by back-reflection Läue X-ray diffraction as described above. The same crystal goniometer stage was used in both the X-ray camera and spark machine to ensure that each disc was precisely aligned. In all spark machining, the voltage was low in order to prevent specimen damage.

Discs were prepared for electron-metallographic examination by jet-electropolishing in solutions of 80/20 methanol/perchloric acid at 40 V and 293 K for Al–Al_3Ni, and 40/30/20/10 water/acetic acid/phosphoric acid/nitric acid at 80 V and 293 K for Al–Al_2Cu. Thin foils produced by this technique were subjected to a preliminary examination in a Philips EM300 electron microscope. Those foils which contained no etched interphase boundaries and no bend contours were used for subsequent examination of dislocation structures in the EM300 microscope, using a tilt-rotation stage with 45° tilt and 360° rotation.

Three experiments were carried out on each foil. First, the crystallography of each foil was determined by Kikuchi-line methods [8] in order to determine the nature and extent of any crystallographic effects of deformation. Second, the dislocation density in the aluminium phase was measured in at least eight areas of each foil. This was achieved by taking bright-field electron micrographs of each area under simple two-beam conditions, counting the number of dislocation/foil surface intersections n_d in an area A, and using the formula [9, 10];

$$\rho = n_d m^2 c / 2A$$

where ρ is the dislocation density, m is the linear magnification, and c is a factor to allow for the

proportion of invisible dislocations under a particular two-beam condition. This factor can be calculated on the assumption that all dislocations are $a/2\langle 110\rangle$ type and tabulated values are given by Hirsch *et al.* [9]. The magnification was determined by putting on each foil a drop of methanol suspension of latex balls of known size. There were several possible counting errors in this method of determining dislocation densities, particularly due to dislocation intersections with interphase boundaries. When the number of dislocation intersections was ambiguous the lowest number was always counted, so the measured dislocation densities may have been consistently low. In those specimens where the dislocations in the aluminium were partly arranged in sub-boundaries, the dislocation density was determined excluding the sub-boundary dislocations.

Third, the detailed nature of dislocation structures was determined by conventional Burgers vector analysis in several areas of each foil. Each area was observed under three or four different two-beam conditions in order to obtain extinction criteria for dislocations in that area [9]. Burgers vectors so obtained were correlated with foil orientations to determine the screw or edge nature of each dislocation.

Detailed dislocation studies were confined to the aluminium phase only, because dislocations were never observed in the Al_3Ni phase, and it was not possible to achieve good two-beam contrast conditions in the Al_2Cu phase. Dislocation densities and Burgers vectors were always determined in the thickest regions of foils, because near foil edges some dislocations were removed during specimen preparation. Some foils, approximately 1 μm thick, were examined in a high energy electron microscope at 750 kV. This demonstrated that dislocation structures observed in the conventional electron microscope were representative of the bulk material.

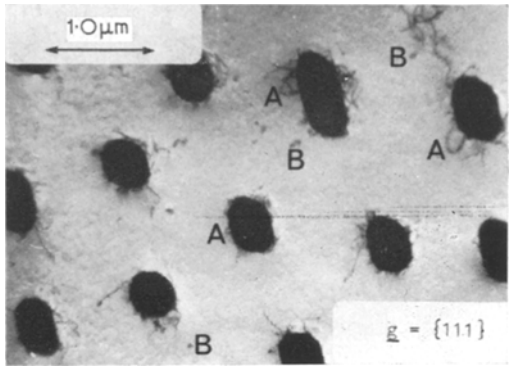

Figure 1 Electron micrograph of a transverse section of as-grown Al–Al_3Ni showing semicircular dislocation segments in the matrix close to interphase boundaries (e.g. at A) and dislocation loops (e.g. at B).

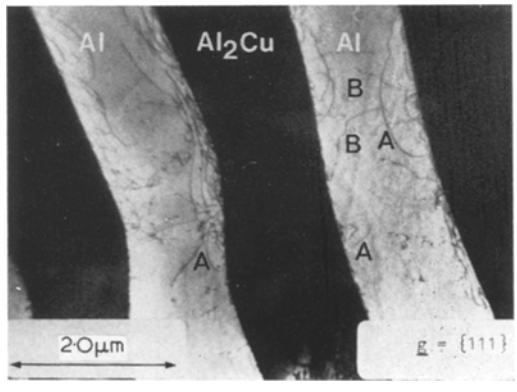

Figure 2 Electron micrograph of a transverse section of as-grown Al–Al_2Cu showing semicircular dislocation segments in the matrix close to interphase boundaries (e.g. at A) and dislocation loops (e.g. at B).

3. Results

3.1. Dislocation structures in the as-grown eutectics

For both Al–Al_3Ni and Al–Al_2Cu, the dislocation density of the as-grown eutectic was surprisingly high, approximately 2 to 3 $\times$ 10^9 dislocation lines per cm^2. Most of the dislocations were in the form of short semicircular segments with both ends terminating at the same interphase boundary (positions A, Figs. 1 and 2). The dislocations were therefore concentrated in interphase boundary regions. There were also a few dislocation loops between the fibres or lamellae of the intermetallic phase (positions B, Figs. 1 and 2). On a scale greater than the interparticle spacing these dislocations structures were homogeneous. Analysis showed that all the dislocations had $a/2\langle 110\rangle$ Burgers vectors. Most of the dislocations were glissile on planes at 30° to 50° to the growth direction although some of the loops were prismatic.

In Al–Al_2Cu, additional dislocations were present at lamellar faults in the form of sub-boundaries in both phases. These were not included in the dislocation density measurements. Lamellar faults were not always associated with crystallographic rotations of the two phases.

When there was crystallographic rotation across a fault, a dislocation sub-boundary was also present. At some lamellar faults there was a sub-boundary in one of the phases but not the other, and there was a corresponding crystallographic rotation in that one phase only. The sub-boundaries were usually composed of a cross-grid of two or three sets of dislocations (see for example Fig. 3). Analysis of aluminium sub-boundaries showed that the dislocations could be pure edge, pure screw, or mixed. The corresponding analysis of Al_2Cu sub-boundaries was not performed. The dislocations present in sub-boundaries were consistent with crystallographic misorientations of 2° to 4°, in agreement with values previously determined [8].

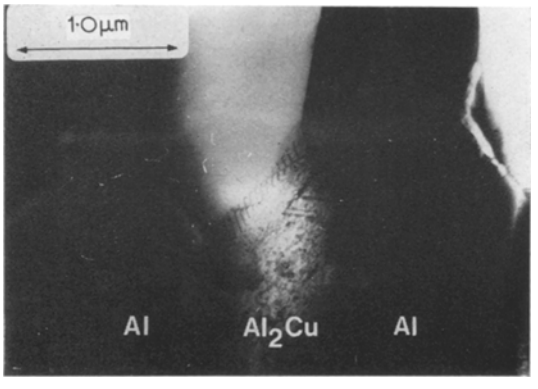

Figure 3 Electron micrograph of a transverse section of as-grown Al – Al_2Cu showing a dislocation sub-boundary in the Al_2Cu phase.

3.2. Stress-strain behaviour

The stress-strain curves of Al–Al_3Ni and Al–Al_2Cu eutectics are shown in Figs. 4 and 5 respectively. Tensile strengths and failure strains for both eutectics at each testing temperature are given in Table I. At 293 and 593 K, Al–Al_3Ni specimens failed at the UTS. At 743 K, plastic instability developed at the UTS after which the stress gradually decreased to zero. Cantor *et al.* [1] have shown that the region of the stress-strain curve in which the gradient is negative is caused by fibre pull-out. At 293 K Al–Al_2Cu specimens failed at the UTS. However, at higher testing temperatures plastic instability was exhibited and specimens failed with the stress decreasing to zero. This has been ascribed to high temperature ductility of the Al_2Cu phase [1]. For both eutectics, the transition from elastic/elastic to

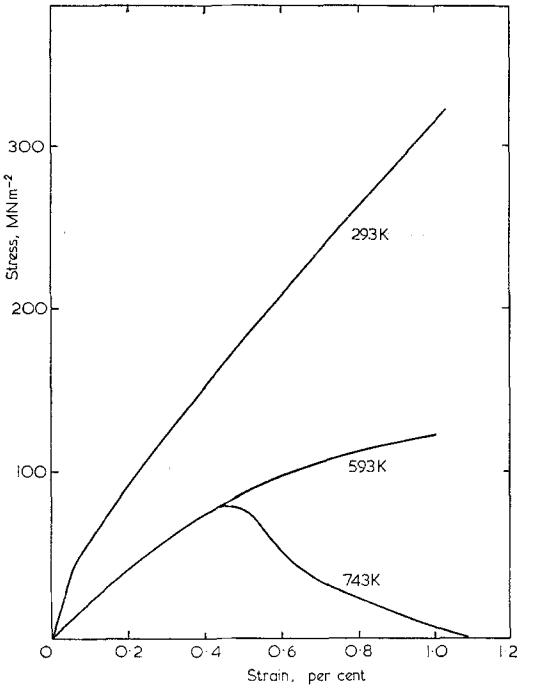

Figure 4 Stress-strain behaviour of Al–Al_3Ni eutectic single crystals deformed in tension at 293, 593 and 743 K.

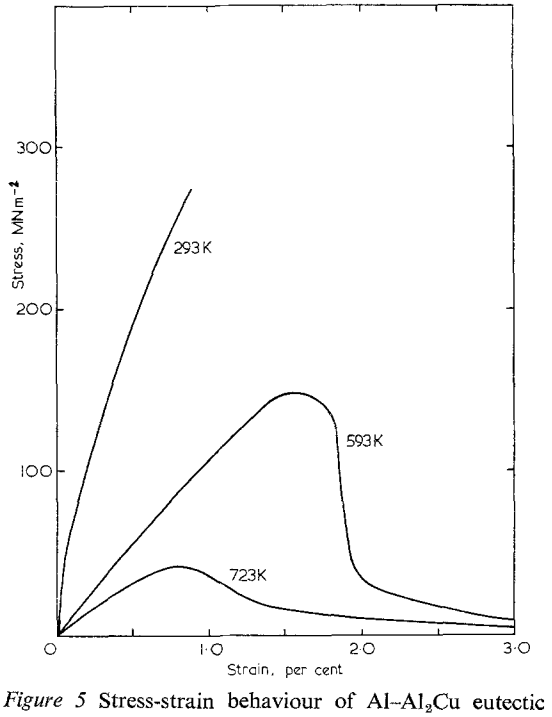

Figure 5 Stress-strain behaviour of Al–Al_2Cu eutectic single crystals deformed in tension at 293, 593 and 723 K.

elastic/plastic behaviour (i.e. composite yield point) was only detected at 293 K. The measured

TABLE I Tensile stress-strain data for Al–Al_3Ni and Al–Al_2Cu eutectics.

Material	Testing temperature (K)	UTS (MN m^{-2})	Failure strain (%)
Al–Al_3Ni	293	321	1.0
	593	123	1.0
	743	81	1.0
Al–Al_2Cu	293	276	0.87
	593	157	4.1
	723	43	4.9

TABLE II Composite yield data for Al–Al_3Ni and Al–Al_2Cu eutectics tested at 293 K

Material	Composite yield strength (MN m^{-2})	Composite yield strain (%)	Composite Young's modulus (GN m^{-2})
Al–Al_3Ni	45	0.06	82.5
Al–Al_2Cu	47	0.06	76.8

yield stresses, yield strains and Young's moduli (i.e. elastic/elastic moduli) at this temperature are presented in Table II.

The stress-strain behaviour of the two eutectics was in approximate agreement with previous data [11-14], with the exception of the high temperature failure strains in Al–Al_2Cu. This discrepancy has been ascribed to a strain rate effect [1]. The eutectic stress-strain behaviour at 293 K was also in agreement with the law of mixtures:

$$E_c = V_F E_F + V_M E_M \quad (1)$$

$$\sigma_c = V_F \sigma_F + V_M \sigma_M \quad (2)$$

where E_c, E_F, E_M are Young's moduli of composite, reinforcing phase and matrix, σ_c, σ_F are fracture stresses of composite and reinforcing phase, σ_M is the matrix stress at the composite fracture point, and V_F, $V_M (= 1 - V_F)$ are the volume fractions of reinforcing phase and matrix. Table III shows values of V_F, E_F and E_M previously reported for the two eutectics and composite moduli calculated from these values using Equation 1. These calculated moduli compare well with the measured values in Table II. It was not possible to determine the extent of agreement with the law of mixtures at higher testing temperatures, because the relevant stress-strain data for Al_3Ni and Al_2Cu are not available.

3.3. Crystallography of deformation

Both X-ray and electron diffraction showed that all crystallographic features of the two eutectics remained constant during deformation irrespective of testing temperature. Although the aluminium phase in all Al–Al_2Cu specimens and some Al–Al_3Ni specimens was oriented for single slip, no crystallographic rotation was observed. With a single slip system operating, the amount of crystallographic rotation of the tensile axis θ, at a strain ϵ, is given by:

$$\sec \theta = 1 + \epsilon .$$

A strain of 1% would produce a rotation of 8°, considerably greater than experimental error. Therefore, multiple slip was operating at all stages of deformation of both eutectics.

3.4. Surface slip line structure

On none of the replicas taken was any surface slip line structure observed. This was the case for both eutectics irrespective of testing temperature and implied that dislocations had not been able to penetrate the thin film of aluminium oxide present on electropolished surfaces of aluminium. Thus no slip plane had sustained extensive dislocation motion and the spacing of active slip planes was quite small.

3.5. Dislocation structures in the deformed eutectics

For both Al–Al_3Ni and Al–Al_2Cu eutectics, the matrix dislocation density was plotted as a function of tensile strain during deformation at three temperatures (Figs. 6 and 7). The results obtained were reproducible, indicating that in all cases dislocations were homogeneously distributed in the matrix.

TABLE III Calculated composite moduli of Al–Al_3Ni and Al–Al_2Cu eutectics tested at 293 K

Material	Volume fraction reinforcing phase	Modulus of reinforcing phase (GN m^{-2})	Matrix modulus (GN m^{-2})	Calculated composite modulus (GN m^{-2})
Al–Al_3Ni	0.1 [11]	137.9 [11]	75.2 [6]	81.5
Al–Al_2Cu	0.475 [6]	94.5 [30]	75.2 [6]	82.4

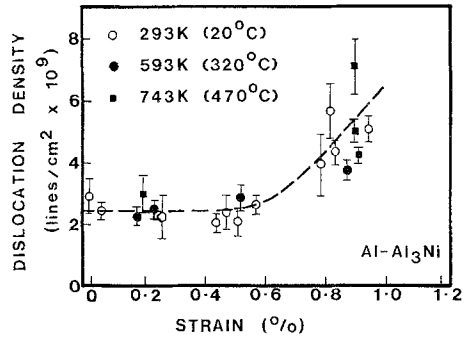

Figure 6 Dislocation density as a function of strain during tensile deformation of Al–Al_3Ni eutectic single crystals.

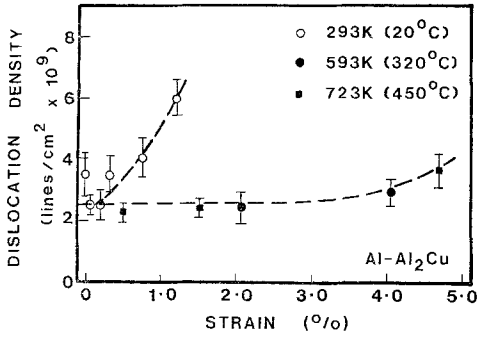

Figure 7 Dislocation density as a function of strain during tensile deformation of Al–Al_2Cu eutectic single crystals.

The matrix dislocation density in Al–Al_3Ni increased from 2 to 3 × 10^9 dislocation lines per cm^2 in the undeformed eutectic, to 7 to 8 × 10^9 dislocation lines per cm^2 after 1% strain, just before fracture, at any of the three testing temperatures. Matrix dislocation structures were also similar at all testing temperatures and independent of foil plane. In the early stages of deformation, arrays of dislocations similar to those in the as-grown eutectic were punched out from fibre-matrix interfaces (Fig. 8). These dislocation arrays propagated between fibres (Fig. 9), and interacted to form tangled networks characteristic of the later stages of deformation (Fig. 10). The number of dislocation loops was slightly greater than that found in the undeformed eutectic. Dislocation pile-ups at fibre-matrix boundaries were occasionally observed in specimens deformed at the higher testing temperatures.

Burgers vector analysis showed that dislocations were predominantly $a/2\langle 110\rangle$ type. Dislocation sub-boundaries were observed in

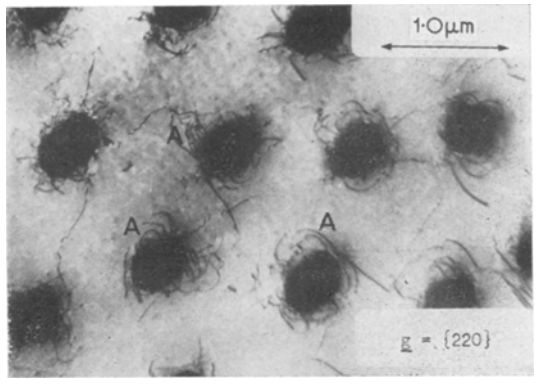

Figure 8 Electron micrograph of a transverse section of Al–Al_3Ni deformed 0.2% in tension at 593 K. Arrays of matrix dislocations are being punched out at interphase boundaries (e.g. at A).

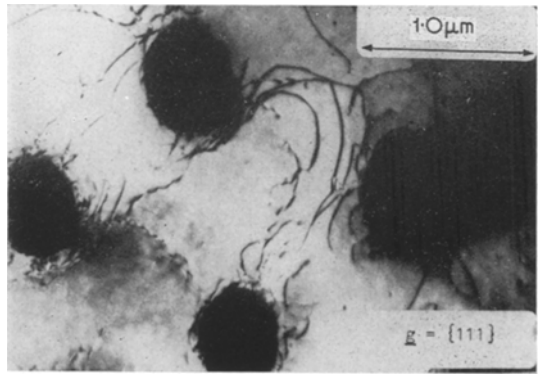

Figure 9 Electron micrograph of a transverse section of Al–Al_3Ni deformed 0.8% in tension at 743 K. Matrix dislocations are propagating between fibres.

only one foil which was taken very close to the fracture surface of a specimen tested at 743 K (Fig. 11). The cell size was approximately equal to the interfibre spacing. It was assumed that this was a region of high local strain due to crack propagation during fracture. Analysis showed that the sub-boundaries consisted of arrays of dislocations which were often pure edge or pure screw and were characteristically associated with 2° to 3° of tilt or twist. Dislocations were never observed in the Al_3Ni phase.

In Al–Al_2Cu deformed at 293 K, the density and structure of matrix dislocations were similar to those found in Al–Al_3Ni. After 1% strain, just before fracture, the matrix dislocation density had increased to 7 to 8 × 10^9 dislocation lines per cm^2, and the dislocations were in

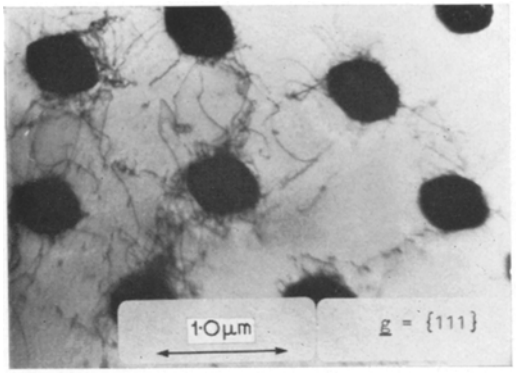

Figure 10 Electron micrograph of a transverse section of Al–Al_3Ni deformed 1.0% in tension at 293 K. Matrix dislocations are in the form of tangled networks between fibres.

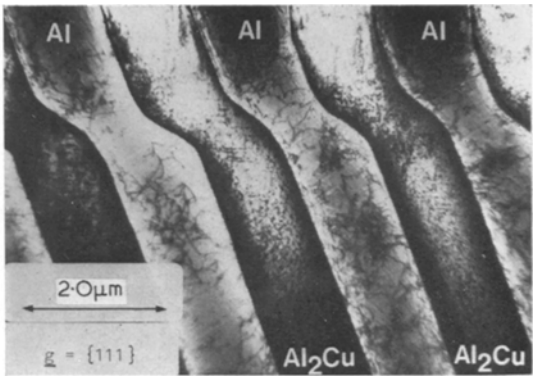

Figure 12 Electron micrograph of a transverse section of Al–Al_2Cu deformed 1% in tension at 293 K. Matrix dislocations are in the form of tangled networks between lamellae.

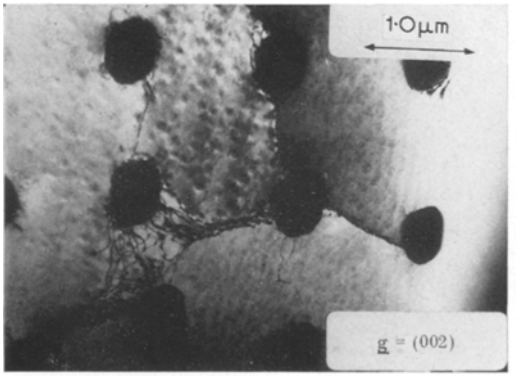

Figure 11 Electron micrograph of a transverse section close to the fracture surface of an Al–Al_3Ni single crystal deformed 1% in tension at 743 K. Matrix dislocations are in the form of sub-boundaries.

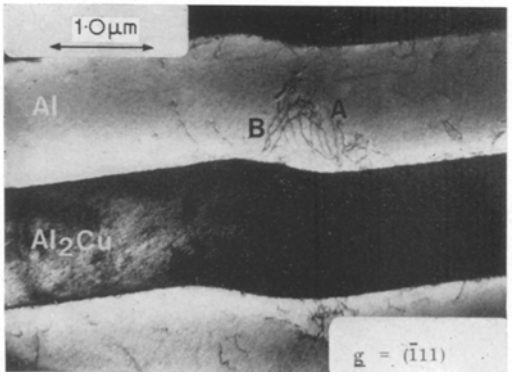

Figure 13 Electron micrograph of a transverse section of Al–Al_2Cu deformed 1% in tension at 293 K. Two arrays of matrix dislocations (A and B) are interacting to form a dislocation network.

tangled networks between Al_2Cu lamellae (Fig. 12). In the earlier stages of deformation, dislocations were punched out at interphase boundaries, propagated between lamellae, and interatced to form networks (Fig. 13). The dislocations had Burgers vectors of the $a/2\langle 110\rangle$ type.

At 593 and 723 K, failure strains in Al–Al_2Cu were 4 to 6% and many of the matrix dislocations were in the form of sub-boundaries (Fig. 14). During deformation, the density of dislocations (excluding those in sub-boundaries) remained constant at 2 to 3 $\times$ 10^9 dislocation lines per cm^2. Plastic strain was presumably accommodated by dislocations forming at lamellar interfaces and propagating into the cell walls. The cellular sub-boundaries consisted of simple edge or screw dislocation arrays associated with 2° to 3° of tilt or twist. The cell size was of the order of the interlamellar spacing. At 593 K there was some evidence of plastic deformation of the Al_2Cu phase, and at 723 K dislocation sub-boundaries were present in the Al_2Cu phase as well as the matrix.

4. Discussion

4.1. Dislocation structures in the as-grown eutectics

The matrix dislocation densities in the two as-grown eutectics are considerably higher than would be expected for single phase materials [15]. Moreover, the dislocation counting pro-

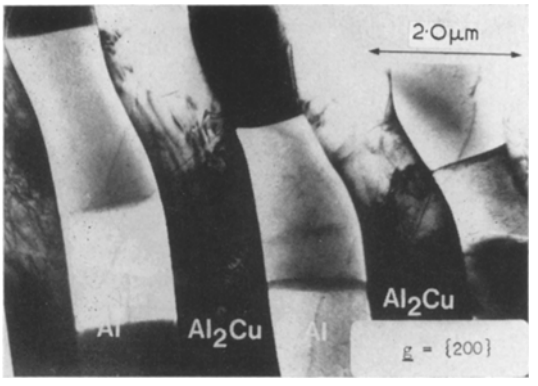

Figure 14 Electron micrograph of a transverse section of Al–Al_2Cu deformed 2% in tension at 593 K. Matrix dislocations are predominantly in the form of sub-boundaries.

cedures were such that results were likely to be low rather than high, and removal rather than introduction of dislocations was the problem encountered in foil preparation. The high dislocation densities are probably due to post-solidification differential thermal contraction stresses. Residual stresses in composites have been analysed in detail [16], and their effect on the mechanical properties of eutectics has also been investigated [6, 17].

Consider a fibre eutectic in which the matrix phase has a greater thermal expansion coefficient than the fibres. On cooling, both phases will be in tension perpendicular to the fibre axis; the matrix will be in tension and the fibres in compression parallel to the fibre axis. To a first approximation, non-axial stresses can be neglected, and the residual axial stresses in the two phases are given by [18]:

$$\sigma_M^R = \frac{V_F E_F E_M}{V_F E_F + V_M E_M} (\alpha_M - \alpha_F)\Delta T \quad (3)$$

$$\sigma_F^R = \frac{V_M E_F E_M}{V_F E_F + V_M E_M} (\alpha_F - \alpha_M)\Delta T \quad (4)$$

where α_M, α_F are the coefficients of linear thermal expansion of the matrix and fibre, and ΔT is the temperature range. For a lamellar eutectic similar equations can be derived with the Young's modulus of each phase replaced by $E/(1 - \nu)$ where ν is Poisson's ratio for that phase. The mean coefficients of thermal expansion for Al_2Cu and aluminium are 20×10^6 and 27×10^6 K^{-1} respectively between 273 and 773 K [19]. For Al–Al_2Cu between room temperature and the eutectic temperature (821 K) [20] there is a temperature range of approximately 520 K. Using the data in Table III and taking $\nu_{Al} = \nu_{Al_2Cu} = 0.33$, Equation 3 predicts a matrix residual tensile stress of 223 MN m^{-2}.

In the absence of residual stresses, the composite yield stress σ_c^Y is determined by the stress at which the matrix yields, σ_M^Y, and can be derived from the law of mixtures [17]:

$$\sigma_c^Y = (V_M + V_F E_F E_M^{-1})\sigma_M^Y . \quad (5)$$

When matrix residual stresses are present, this is modified to:

$$\sigma_c^Y = (V_M + V_F E_F E_M^{-1})(\sigma_M^Y \pm \sigma_M^R) \quad (6)$$

where $+ \sigma_M^R$ and $- \sigma_M^R$ refer to the compression and tensile composite yield stresses respectively [17]. Pattnaik and Lawley [6] have measured the compression and tensile yield stresses of Al–Al_2Cu and obtained a matrix residual tensile stress of 24 MN m^{-2} from Equation 6. This value is an order of magnitude lower than that calculated from expansion coefficients and this may be due to neglecting non-axial stresses or inaccuracies in the expansion coefficient data. A more probable explanation is that much of the matrix residual stress is removed by creep at high temperatures. As in the present work, Pattnaik and Lawley's eutectics were grown as single crystals and therefore only very slowly cooled to room temperature after solidification. Considerable stress relaxation would be expected to occur during this slow cooling.

There is no evidence for the presence of GP zones or precipitates in the matrix phase of Al–Al_2Cu, therefore this phase consists of an equilibrium solid solution of aluminium – 0.04 wt % copper [20]. The yield stress of 99.999% pure as-solidified aluminium single crystals is $\sim$ 1.5 MN m^{-2} [21]; that of aluminium – 4.5 wt % copper single crystals is $\sim$ 40 MN m^{-2} [22]. These quoted yield stresses both refer to orientations close to the growth direction of aluminium in Al-Al_2Cu. Interpolating, the matrix yield stress should be no greater than $\sim$ 2.0 MN m^{-2}, although this will be increased by the constraint effect of closely spaced fibres (discussed later).

Residual stress levels are sufficient to cause considerable plastic flow in the matrix and account for the high matrix dislocation densities observed in the as-grown eutectic. It should also be noted that dislocations are predominantly

concentrated in interface regions where residual stresses are greatest.

4.2. Micromechanics of deformation

During eutectic deformation glissile grown-in dislocations begin to move, and more dislocations are created at interphase boundaries. In this way, arrays of dislocations propagate from interphase boundaries into the matrix and interact to form tangled dislocation networks. The creation of dislocations produces an increase in the matrix dislocation density. In general, with matrix strains below 1% throughout the deformation process, dislocation sub-boundaries are not formed and dislocation pile-ups at interphase boundaries are rare. However, sub-boundaries are readily formed in Al–Al_2Cu tested at higher temperatures where failure strains are 4 to 5%, and are also observed in regions of locally high strain close to fracture surfaces.

If a material containing a density of dislocations ρ of Burgers vector $\boldsymbol{b}$ is strained so that each dislocation moves a distance x, the strain produced is:

$$\epsilon = \rho \boldsymbol{b} x \,.$$

For a strain of 1%, initial dislocation density of 3×10^9 dislocation lines per cm^2 and Burgers vector of 2 Å, each dislocation slips a distance of 1.7 μm. For a strain of 5%, the dislocation slip distance is 8.3 μm. For Al–Al_3Ni and Al–Al_2Cu, the dislocation density increases by a factor of $\sim$ 2.5 during the deformation, therefore the slip distances are closer to 0.7 and 3.2 μm for 1 and 5% strain respectively. Therefore, in Al–Al_3Ni at all temperatures and Al–Al_2Cu at 293 K, dislocation slip distances are no greater than half the interlamellar spacing. For this reason, there is insufficient dislocation interaction for sub-boundary formation to take place. In Al–Al_2Cu tested at higher temperatures and in local regions close to fracture surfaces, the total plastic strain is greater and dislocation slip distances are large enough for the formation of dislocation sub-boundaries (Figs. 11 and 14). For the Al–Al_2Cu tested at higher temperatures this may be predominantly by dislocation climb. However, in local regions of high strain at low testing temperatures, the sub-boundaries must form by cross-slip which is relatively easy in aluminium because of its high stacking fault energy.

Dislocation sub-boundaries have been observed in Al–Al_3Ni and Al–Al_2Cu eutectics deformed at 293 K by Gould and Martin [4] and Pattnaik and Lawley [6] respectively. In the latter case, sub-boundaries were presumably either in isolated regions of locally high strain, or caused by dislocations introduced during specimen handling. Gould and Martin [4] claim to have removed grown-in dislocations by annealing Al–Al_3Ni specimens before tensile testing. With a smaller initial dislocation density, slip distances could be greater and sub-boundaries would form during deformation. However, differential thermal contraction stresses must be produced on cooling from the annealing temperature. The magnitude of these residual stresses, even over a reduced temperature range, is likely to cause matrix plastic flow and reintroduce matrix dislocations. Therefore, it is not yet clear to what extent matrix dislocations can be removed by annealing treatments.

From Equation 6 it is possible to obtain the stress at which the matrix yields in the composite as:

$$\sigma_M{}^Y = \frac{\sigma_c{}^Y E_M}{V_M E_M + V_F E_F} \pm \sigma_M{}^R \,. \qquad (7)$$

Using the measured composite yield stresses from Table II, data from Table III, the Al–Al_2Cu matrix residual stress measured by Pattnaik and Lawley [6], and assuming a similar residual stress in Al–Al_3Ni, $\sigma_M{}^Y$ is 65.5 MN m^{-2} and 64.5 MN m^{-2} for Al–Al_3Ni and Al–Al_2Cu respectively. The matrix phases in the two eutectics consist of Al–0.006 wt % Ni and Al–0.04 wt % Cu [20], and their yield stresses alone are approximately 1.5 and 2.0 MN m^{-2} respectively (see previous section). The yield stress of the aluminium matrix is increased in each eutectic by more than an order of magnitude, simply due to the presence of the reinforcing phase.

The matrix yield stress in each composite is considerably greater than the yield stress of the same material without the presence of a reinforcing phase. This effect has been observed in conventional fibre-reinforced composites with small interfibre spacings [23-25], and also in eutectic composites [26]. The same workers have also observed composite work-hardening rates greater than those expected from the law of mixtures. Kelly and Lilholt [24] have suggested that matrix deformation is inhibited by a triaxial stress state caused by differential lateral contraction of the two composite phases. Neumann and Haasen [27] have provided an alternative

explanation in which the matrix constraint is provided by dislocation pile-ups at fibre-matrix interfaces.

On Kelly and Lilholt's model, initial yielding of the matrix should occur in those regions most distant from fibre-matrix interfaces where lateral stresses are least. As shown in the present work, however, matrix yielding in Al–Al_3Ni and Al–Al_2Cu is initiated close to interphase boundaries as has been predicted previously [26]. This is due to the presence of glissile grown-in dislocations in the interface regions. The dislocation pile-up model [27] is also not applicable to Al–Al_3Ni or Al–Al_2Cu because dislocation slip distances are insufficient for extensive pile-ups to form. However, the intermetallic fibres or lamellae will cause back-stresses on dislocation sources in a similar fashion to back-stresses caused by pile-ups and this may explain the constraint effect for the two eutectics.

Ashby [28] has pointed out that to maintain strain compatibility during deformation of a composite, one of two things takes place. Either the matrix deforms by multiple slip, or alternatively, geometrically necessary dislocations are introduced into the matrix to compensate for undeformed second phase particles. In the latter case, the geometrically necessary dislocations may be in any one of many configurations, but the two common configurations are shear loops around second phase particles, and prismatic loops caused by cross-slip [29]. Geometrically necessary dislocations are formed when the stress required for their formation is less than that required to initiate multiple slip. According to Ashby's calculations, the formation of geometrically necessary dislocations should be a common phenomenon at low strains. This is because the stress required to create new dislocations on secondary slip planes and thus initiate multiple slip, is usually relatively high. However, if the interface between the two phases is weak and incoherent or if dislocation sources are available close to the interface, then multiple slip is initiated quite readily and geometrically necessary dislocations are not formed.

Laue X-ray data show that there is no bulk crystallographic rotation during deformation of Al–Al_3Ni or Al–Al_2Cu, irrespective of matrix orientation. This implies that multiple slip is initiated at the yield point in both eutectics. Both electron diffraction data and the lack of asterism on Läue X-ray patterns show that there is no local crystallographic rotation during deformation. Therefore, shear loops are not formed around eutectic fibres or lamellae. Moreover, bright-field electron micrographs show no evidence of the formation of either shear loops or prismatic loops in either eutectic. The prismatic loop configuration of geometrically necessary dislocations is relatively unfavourable for second phase particles with large aspect ratios [28].

In both eutectics, multiple slip is initiated at the yield point and geometrically necessary dislocations are not formed. The eutectic interfaces are certainly not weak although not fully coherent [8]. However, grown-in dislocations are readily available on secondary slip planes in the interface region, and at positions where grown-in dislocations have interacted there are potential dislocation sources. Therefore, because of the presence of grown-in dislocations, multiple slip is initiated at the yield point.

5. Conclusions

In as-solidified single crystals of Al–Al_3Ni and Al–Al_2Cu eutectics the matrix dislocation density is high, $\sim$ 2 to 3 $\times$ 10^9 dislocation lines per cm^2. The dislocations are concentrated in interphase boundary regions and are formed by post-solidification differential thermal contraction stresses.

The tensile deformation of the two eutectics is controlled by two main features: the constraint effect of closely spaced fibres or lamellae, and the high initial dislocation density. Eutectic yield stresses and work-hardening rates are high due to the constraint effect. Because of the high initial dislocation density, multiple slip is initiated at the yield point and no crystallographic rotation occurs during deformation. On yielding, large numbers of glissile grown-in dislocations propagate through the matrix and new dislocations are created at interphase boundaries. In Al–Al_3Ni deformed at all temperatures and Al–Al_2Cu deformed at room temperature, failure strains are approximately 1%, dislocation slip distances are small, and tangled dislocation networks are formed. In Al–Al_2Cu deformed at higher temperatures, failure strains are greater because the Al_2Cu phase is ductile; slip distances are therefore greater, and dislocation sub-boundaries can be formed, sometimes in both phases. Dislocation sub-boundaries are also produced in regions of locally high strain close to fracture surfaces.

References

1. B. CANTOR, G. J. MAY and G. A. CHADWICK, *J. Mater. Sci.* **8** (1973) 830.
2. G. J. MAY and G. A. CHADWICK, *Met. Sci. J.* **7** (1973) 20.
3. F. D. LEMKEY and E. R. THOMPSON, *Met. Trans.* **2** (1971) 1537.
4. D. GOULD and J. W. MARTIN, Proceedings of the Conference on *In Situ* Composites, (Lakeville 1972, NMAB 308).
5. E. M. BREINAN, E. R. THOMPSON and W. K. TICE, *Met. Trans.* **3** (1972) 211.
6. A. PATTNAIK and A. LAWLEY, *Met. Trans.* **2** (1971) 1529.
7. G. A. CHADWICK, *Prog. Mat. Sci.* **12** (1963) 97.
8. B. CANTOR and G. A. CHADWICK, *J. Crystal Growth* **23** (1974) 12.
9. P. B. HIRSCH, A. HOWIE, R. B. NICHOLSON, D. W. PASHLEY and M. J. WHELAN, "Electron Microscopy of Thin Crystals" (Butterworths, London, 1965).
10. R. K. HAM and N. G. SHARPE, *Phil. Mag.* **6** (1961) 1193.
11. R. W. HERTZBERG, F. D. LEMKEY and J. A. FORD, *Trans. Met. Soc. AIME* **233** (1965) 342.
12. M. J. SALKIND, F. D. LEMKEY and F. D. GEORGE, "Whisker Technology", edited by A. P. Levitt (Wiley, New York, 1967) Ch. 10.
13. B. R. BUTCHER, G. C. WEATHERLY and H. R. PETTIT, *Met. Sci. J.* **3** (1969) 7.
14. F. W. CROFFMAN, A. S. YUE and A. E. VIDOZ, *Trans. Met. Soc. AIME* **245** (1969) 397.
15. B. CHALMERS, "Physical Metallurgy" (Wiley, New York, 1959) p. 109.
16. S. S. HECKER, C. H. HAMILTON and L. J. EBERT, *J. Mat.* **5** (1970) 868.
17. D. A. KOSS and S. M. COPLEY, *Met. Trans.* **2** (1971) 1557.
18. F. LASZLO, *JISI* **147** (1943) 173.
19. I. G. DAVIES, D.Phil. Thesis, (Oxford 1969) p. 123.
20. M. HANSEN and K. ANDERKO, "Constitution of Binary Alloys" (McGraw-Hill, New York, 1958).
21. J. T. MCGRATH and G. B. CRAIG, *Trans. Met. Soc. AIME* **215** (1959) 1022.
22. G. GREETHAM and R. W. K. HONEYCOMBE, *JIM* **89** (1960) 13.
23. N. M. PARIKH, "Fibre Composite Materials" (ASM, Cleveland, Ohio, 1965) p. 115.
24. A. KELLY and H. LILHOLT, *Phil. Mag.* **20** (1969) 311.
25. G. GARMONG and L. A. SHEPARD, *Met. Trans.* **2** (1971) 175.
26. A. R. T. DE SILVA and G. A. CHADWICK, *Met. Sci. J.* **3** (1969) 168.
27. P. NEUMANN and P. HAASEN, *Phil. Mag.* **23** (1971) 285.
28. M. ASHBY, *ibid* **21** (1970) 399.
29. P. B. HIRSCH and F. J. HUMPHRIES, "Physics of Strength and Plasticity" edited by A. Argon (MIT Press, Cambridge, Mass., 1969).

Received 1 September and accepted 9 September 1974.